# Reduced synaptic vesicle protein degradation at lysosomes curbs *TBC1D24/sky*-induced neurodegeneration

Ana Clara Fernandes,[1,2]* Valerie Uytterhoeven,[1,2]* Sabine Kuenen,[1,2] Yu-Chun Wang,[1,2] Jan R. Slabbaert,[1,2] Jef Swerts,[1,2] Jaroslaw Kasprowicz,[1,2] Stein Aerts,[2] and Patrik Verstreken[1,2]

[1]VIB Center for the Biology of Disease and [2]Center for Human Genetics Laboratory of Neuronal Communication, KU Leuven, 3000 Leuven, Belgium

Synaptic demise and accumulation of dysfunctional proteins are thought of as common features in neurodegeneration. However, the mechanisms by which synaptic proteins turn over remain elusive. In this paper, we study *Drosophila melanogaster* lacking active TBC1D24/Skywalker (Sky), a protein that in humans causes severe neurodegeneration, epilepsy, and DOOR (deafness, onychdystrophy, osteodystrophy, and mental retardation) syndrome, and identify endosome-to-lysosome trafficking as a mechanism for degradation of synaptic vesicle-associated proteins. In fly *sky* mutants, synaptic vesicles traveled excessively to endosomes. Using chimeric fluorescent timers, we show that synaptic vesicle-associated proteins were younger on average, suggesting that older proteins are more efficiently degraded. Using a genetic screen, we find that reducing endosomal-to-lysosomal trafficking, controlled by the homotypic fusion and vacuole protein sorting (HOPS) complex, rescued the neurotransmission and neurodegeneration defects in *sky* mutants. Consistently, synaptic vesicle proteins were older in HOPS complex mutants, and these mutants also showed reduced neurotransmission. Our findings define a mechanism in which synaptic transmission is facilitated by efficient protein turnover at lysosomes and identify a potential strategy to suppress defects arising from TBC1D24 mutations in humans.

## Introduction

Loss-of-function mutations in human *TBC1D24* cause severe neurodegeneration, focal and infantile myoclonic epilepsy, malignant migrating partial seizures of infancy, intellectual disability, and DOOR (deafness, onychdystrophy, osteodystrophy, and mental retardation) syndrome (Corbett et al., 2010; Falace et al., 2010; Guven and Tolun, 2013; Milh et al., 2013; Campeau et al., 2014). However, the molecular nature of the defects upon loss of *TBC1D24* remains poorly characterized.

*TBC1D24* encodes an evolutionarily conserved GTPase-activating protein (Uytterhoeven et al., 2011). In flies, Skywalker (Sky)/TBC1D24 resides at synapses and inhibits Rab35-mediated synaptic vesicle trafficking in a pathway parallel to Rab5 (Uytterhoeven et al., 2011). Rab5 and Rab35 promote synaptic vesicles to fuse with endosomes, and this additional trafficking step correlates with increased transmitter release and a larger pool of readily releasable vesicles (RRPs; Wucherpfennig et al., 2003; Uytterhoeven et al., 2011). However, it is not clear how fusion of vesicles with endosomes results in increased neurotransmitter release.

We hypothesize that endosomes may serve as sorting stations for synaptic vesicle proteins, whereby dysfunctional synaptic vesicle proteins are removed from the vesicle cycle at endosomes and sent to the lysosome for degradation. When the dysfunctional vesicle proteins are removed from the vesicle cycle, synaptic vesicles would be populated by the remaining functional vesicle proteins, thus facilitating neurotransmission. In an unbiased modifier screen for *sky* mutant phenotypes, we identified a homotypic fusion and vacuole protein sorting (HOPS) complex component Deep orange (Dor)/VPS18, which has been

*A.C. Fernandes and V. Uytterhoeven contributed equally to this paper.

Correspondence to Patrik Verstreken: patrik.verstreken@med.kuleuven.be

Abbreviations used in this paper: ANOVA, analysis of variance; CSP, cysteine string protein; Dor, Deep orange; EJC, excitatory junctional current; EMS, ethyl methanesulfonate; ERG, electroretinogram; FT, fluorescent timer; HOPS, homotypic fusion and vacuole protein sorting; mEJC, miniature EJC; NMJ, neuromuscular junction; nSyb, neuronal synaptobrevin; Sky, Skywalker; SNP, single nucleotide polymorphism; TEM, transmission EM; Ub, ubiquitin.



The Rockefeller University Press $30.00
J. Cell Biol. Vol. 207 No. 4 453–462
www.jcb.org/cgi/doi/10.1083/jcb.201406026

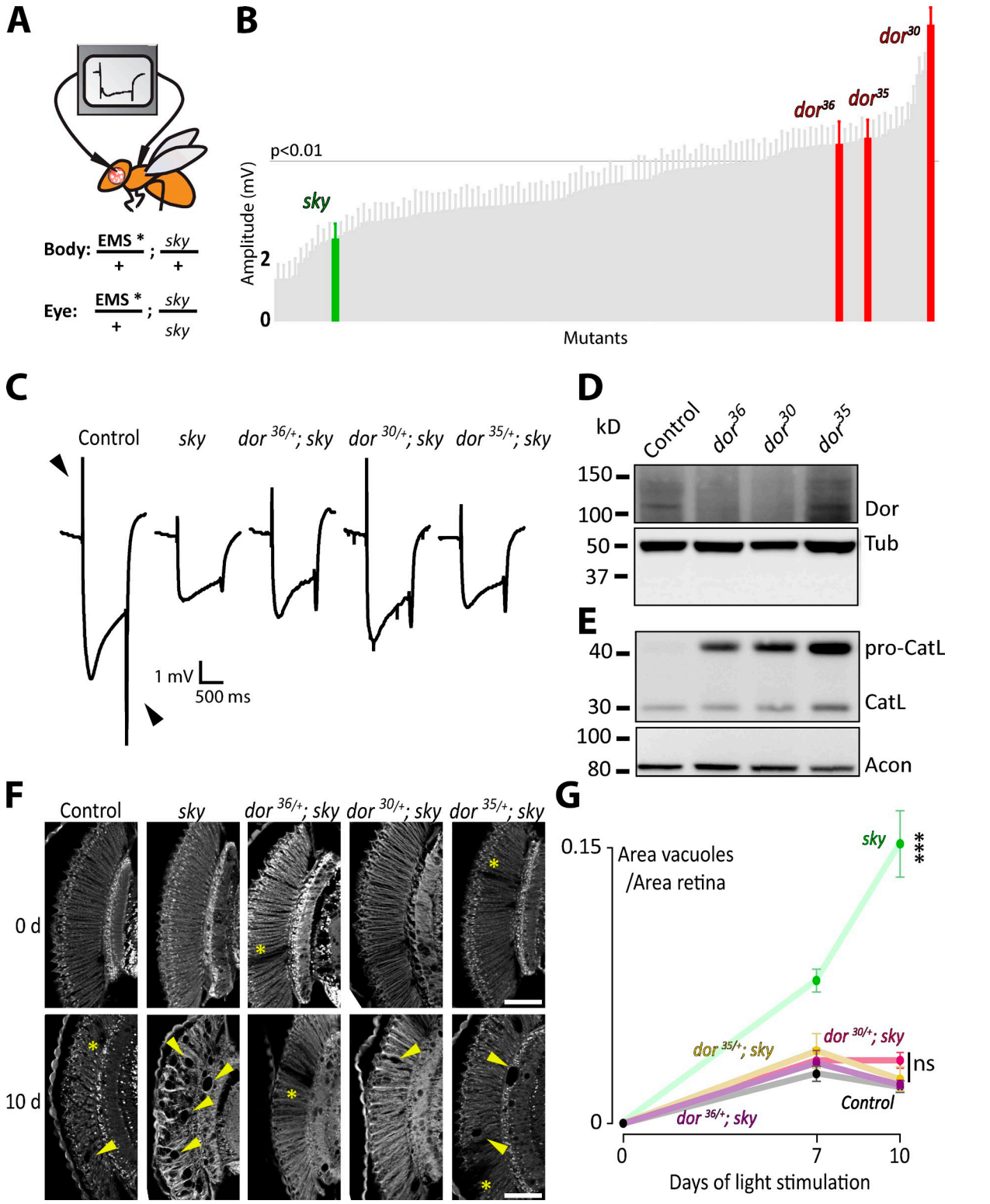


Figure 1. **Heterozygous loss of *dor/VPS18* suppresses *sky/TBC1D24*-induced neurodegeneration.** (A) Schematic representation of ERG recordings to isolate *sky* suppressors. Genotypes in the eye and the rest of the body. (B) Quantification of the sum of the on and off transients in ERG recordings (arrowheads in C) of the screened flies. Amplitudes of *sky* and *dor/+; sky*$^{2}$ are indicated. ($n$ = 3–18.) Error bars: SEM. One-way analysis of variance (ANOVA; post hoc Dunnett's test). (C) Mean ERGs recorded from 5–12 flies with the following genotypes in the eyes: FRT40A (control), *sky*$^{2}$, *dor*$^{36/+}$*; sky*$^{2}$, *dor*$^{30/+}$*; sky*$^{2}$, and *dor*$^{35/+}$*; sky*$^{2}$. Note the partial rescue of on and off transient amplitude defect in *sky*$^{2}$ mutants when *dor* is heterozygous. (D) Western blot to assess Dor levels in homozygous *dor* mutant larvae using anti-Dor and anti–α-Tubulin (Tub) antibodies. ($n$ = 3.) (E) Western blot of *dor* mutants, using anti–insect Cathepsin L (CatL) and anti-Acon. ($n$ = 3.) (F and G) Retina sections of flies with FRT40A (control), *sky*$^{2}$, and *dor*$^{+/-}$*; sky*$^{2}$ mutant eyes not exposed to light (0 d) or exposed for 7 (only shown in G) or 10 d to constant light (10 d) and quantification of the area of vacuoles normalized to retina area (G; $n$ = 5–11 sections). Arrowheads indicate vacuoles, and asterisks indicate red pigment clones in the eyes (result of mitotic recombination—see Materials and methods). Bars, 50 µm. Error bars: SEM. One-way ANOVA (post hoc Tukey's test): ***, P < 0.001.

previously described to control endosome-to-lysosomal trafficking (Rieder and Emr, 1997). The HOPS complex consists of Vps11, 16, 18, 33, 39, and 41 and binds to proteins that mediate fusion of cargo vesicles with the lysosome. Using a fluorescent synaptic vesicle-associated timer, we show that the HOPS complex is critical for synaptic vesicle protein turnover. Furthermore, similar to loss of *TBC1D24* in humans, *sky* mutant flies show massive brain lesions reminiscent of neurodegeneration, which can also be rescued by the partial inhibition of Dor. Our work unveils a mechanism by which endosome-to-lysosomal trafficking controls synaptic vesicle protein turnover, ensuring proper levels of neurotransmitter release as well as neuronal survival in the context Sky/TBC1D24 function.

## Results and discussion

### The HOPS complex component *dor* is a *sky* suppressor

Loss of *sky/TBC1D24* in humans causes neurodegeneration and other neuronal defects. To identify genetic modifiers of *sky*, we performed a genetic screen in fruit flies. *Sky* mutants die in development, but flies homozygously mutant for *sky* only in their eyes, survive, and show defects in electroretinograms (ERGs; Uytterhoeven et al., 2011). ERGs measure the difference in potential between the eye and the body during a light flash (Fig. 1 A). *Sky* mutant eyes result in smaller on and off transients in ERG traces, indicating desynchronized neuronal communication (Fig. 1, B and C; Uytterhoeven et al., 2011). To identify dominant modifiers of the *sky* ERG phenotype, we used a previously isolated collection of 111 X-linked mutants (Fig. 1 A). These chemically randomly induced (ethyl methanesulfonate [EMS]) mutations were isolated because they show defects in neurotransmission when homozygous in the eye, and we therefore reasoned they would be good candidates to genetically interact with *sky* (see Materials and methods). We generated flies homozygous in the eye for *sky* and heterozygous for one of the 111 mutations (Fig. 1 A) and recorded ERGs (Stowers and Schwarz, 1999; Newsome et al., 2000). Although most mutants do not affect the *sky*-induced ERG defect, 26 of the 111 mutants show rescue ($P < 0.01$; Fig. 1 B). Interestingly, we isolated three suppressor mutants, $dor^{30}$, $dor^{35}$, and $dor^{36}$ (Fig. 1, B and C) that also fail to complement one another based on lethality, suggesting they are alleles of the same gene.

To identify the genetic lesions in the $dor^{30}$, $dor^{35}$, and $dor^{36}$ mutant alleles, we combined mapping with whole genome sequencing (Fig. S1) and identified a splice donor mutation resulting in a protein with 56 additional amino acids and an early stop codon in the case of $dor^{35}$ and nonsense mutations in $dor^{36}$ and $dor^{30}$ (Fig. S1, A and B). Immunoblotting revealed lower Dor protein levels in $dor^{36}$ and $dor^{30}$ mutants (Fig. 1 D), whereas $dor^{35}$ is still expressed (though is a dysfunctional protein, as outlined in the next paragraph). Thus, these three alleles appear to result in loss of Dor function. In agreement with this, the larval lethality associated with the *dor* alleles can be rescued by ubiquitous expression of Dor (*daGAL4*).

Dor is an orthologue of Vps18, a member of the HOPS complex (Shestopal et al., 1997), which promotes trafficking of vesicles to lysosomes for degradation in yeast (Rieder and Emr, 1997). To assess whether Dor has a similar function in flies, we measured the conversion of the endolysosomal protease Cathepsin L from its proform into mature Cathepsin L in *dor* mutants. Pro–Cathepsin L is delivered to the lysosome by HOPS-dependent transport, in which its propeptide is subsequently cleaved and the protease becomes active (Zhang et al., 2009). Therefore, we would expect that defects in HOPS-dependent transport would result in less Cathepsin L delivery to lysosomes and thus an accumulation of the propeptide in comparison to its mature form. Indeed, we found all *dor* mutants show an accumulation of pro–Cathepsin L (Fig. 1 E, pro-CatL), indicating that Dor is also required for normal lysosomal trafficking in flies.

### *Dor* mutations suppress *sky*-induced neurodegeneration

To assess whether flies with homozygous mutant $sky^2$ retinae constitute a model for *TBC1D24*-induced neurodegeneration, we performed histological analysis. The morphology of the retina of $sky^2$ mutant eyes in 1-d-old flies is very similar to controls. However, in a 10-d period under constant light, many vacuoles accumulate (Fig. 1, F and G). Next, we analyzed retinae that are homozygous for $sky^2$ and heterozygous for the different *dor* alleles. Consistent with the *dor*-dependent rescue of ERG defects, we find an almost complete suppression of the neurodegeneration induced by loss of *sky* (Fig. 1, F and G).

### Reduced *HOPS* function suppresses neurotransmission defects in *sky* mutants

Neurodegeneration is often linked to abnormal synaptic transmission (Fernández-Chacón et al., 2004). Accordingly, *sky* mutants show a significant increase in neurotransmission (Fig. 2, A and B; Uytterhoeven et al., 2011). To determine whether loss of *dor* suppresses the neurotransmission defects in *sky* mutants, we resorted to two-electrode voltage clamp at the larval neuromuscular junction (NMJ). The excitatory junctional current (EJC) in *sky* mutants is 77% larger than in controls, and removing one copy of *dor* suppresses this defect (Fig. 2, A and B). This rescue is specific to loss of *dor* because expression of Dor (*daGAL4*) in *sky*; *dor*/+ mutants likewise results in much larger EJCs (Fig. 2, A and B). These data indicate that Dor down-regulation rescues the increased neurotransmitter release in *sky* mutants.

We previously showed that loss of *sky* causes synaptic vesicles to cycle excessively to endosomes (Uytterhoeven et al., 2011). To assess whether loss of *dor* also suppresses this defect, we incubated larval fillets in FM 1–43 under stimulating conditions, resulting in the uptake of the dye into newly formed vesicles. In *sky* mutants, the dye concentrates in aberrant accumulations (Fig. 2 C), which are positive for the endosomal marker Rab5-GFP (Uytterhoeven et al., 2011), indicative of increased synaptic vesicle trafficking to endosomes. Despite our observation that loss of Dor rescues the increased synaptic transmission in *sky* mutants, the occurrence of Rab5-positive FM 1–43 accumulations persist in *dor*/+; *sky* double mutants (Fig. 2, C and D; and Fig. S2 A). Thus, reduced Dor function can rescue defects in neurotransmitter release but does not prevent vesicles from excessively cycling to endosomal compartments in *sky* mutants.

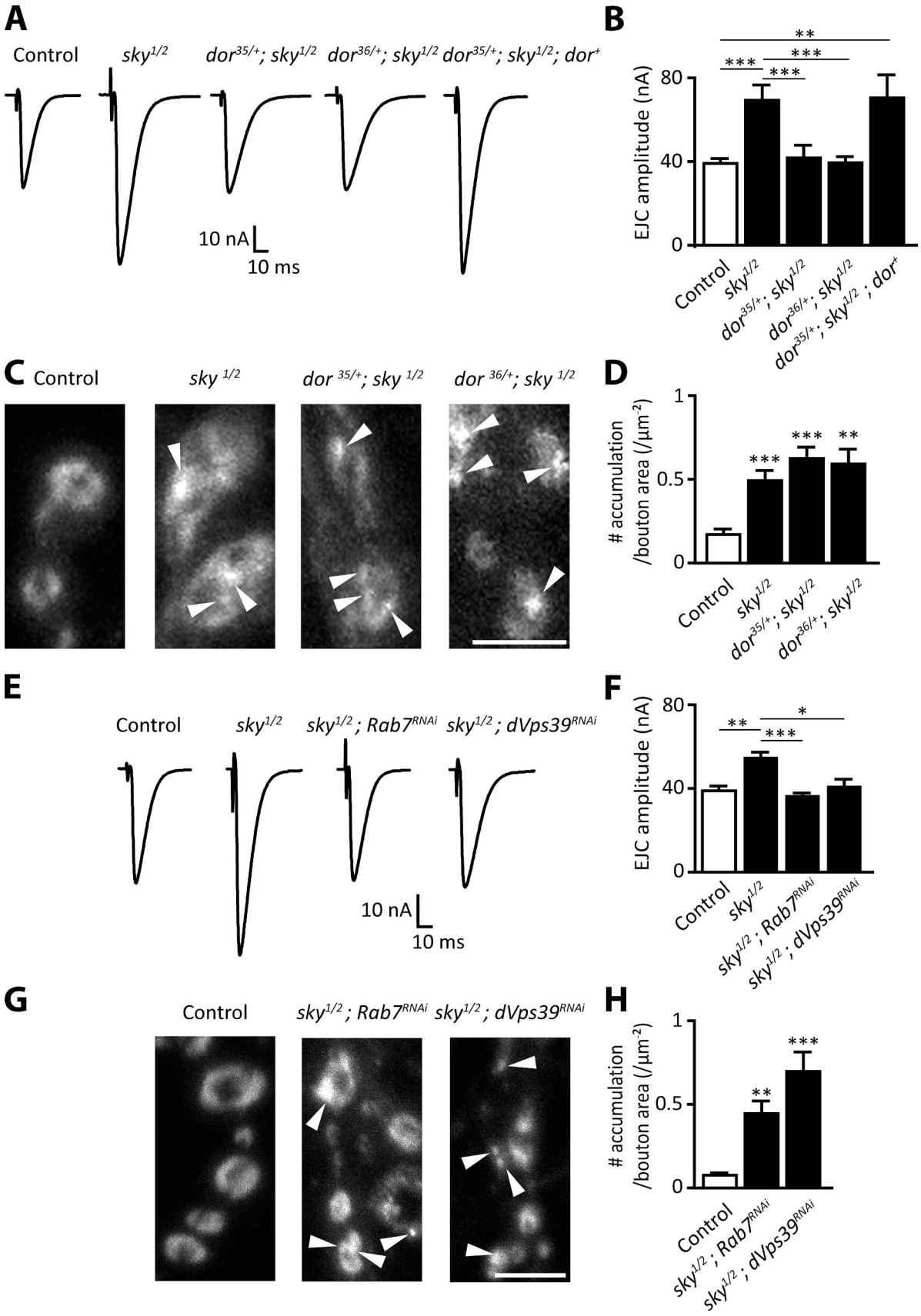


Figure 2. **Reduced endolysosomal trafficking suppresses the increased synaptic transmission defects in *sky* mutants.** (A and B) Traces (A) and quantification (B) of EJC amplitudes recorded from larval fillets in HL3 with 0.5 mM $CaCl_2$ in FRT40A controls, *FRT19A/+; sky*$^{1/2}$ mutants, *dor*$^{35/+}$*; sky*$^{1/2}$, *dor*$^{36/+}$*; sky*$^{1/2}$, and *dor*$^{35/+}$*; sky*$^{1/2}$*; daGAL4 UAS-dor* (*dor*$^{+}$), expressing Dor ubiquitously ($n$ = 5–12). (C and D) Images of FM 1–43 labeling in NMJs on muscle 6

Dor is a member of the HOPS complex and to assess whether other HOPS components or proteins involved in lysosomal trafficking also suppress aspects of the *sky* mutant phenotype, we used the neuronal driver *nSybGAL4* and RNAi to knock down *vps39*/*CG7146* and *rab7* (knockdown efficiency by quantitative RT-PCR: 36% *CG7146* and 40% *rab7*). Similar to partial loss of Dor, RNAi to *vps39* or *rab7* suppresses the increased EJC amplitude in *sky* mutants (Fig. 2, E and F) but not the aberrant accumulations of FM 1–43 (Fig. 2, G and H). These data suggest that trafficking of vesicles to endosomes in *sky* mutants is not sufficient to facilitate neurotransmitter release but that efficient HOPS complex-dependent traffic to lysosomes is required as well.

### *Dor* mutants exhibit defects in synaptic vesicle recycling

To assess the contribution of Dor-dependent lysosomal traffic in exocytosis of synaptic vesicles, we measured the mean amplitude of EJCs and of spontaneous mini-events (miniature EJCs [mEJCs]). Although the mean EJC amplitudes in *dor* mutants and controls are similar (Narayanan et al., 2000), the mEJC amplitudes in both $dor^{35}$ and $dor^{36}$ mutants are larger compared with controls and can be rescued by restoring the expression of Dor ubiquitously (*daGAL4*; Fig. 3, A–D). Hence, the quantal content (EJC/mEJC) in *dor* mutants is reduced compared with controls (Fig. 3 F), suggesting that in *dor* mutants, less vesicles fuse with the synaptic membrane upon nerve stimulation.

Larger mEJCs can originate either from larger vesicles that harbor more neurotransmitters or from increased synaptic glutamate receptor abundance. Quantification of synaptic vesicle diameter using transmission EM (TEM) of $dor^{35}$ and $dor^{36}$ mutant synaptic boutons does not reveal a difference in mean synaptic vesicle size compared with controls (Fig. S2 B). However, $dor^{35}$ and $dor^{36}$ mutants display increased glutamate receptor labeling at synapses (anti-GluRIIA intensity normalized to anti-HRP: control, 1.0 ± 0.10; $dor^{35}$, 1.19 ± 0.13 arbitrary units). These data are therefore consistent with the hypothesis that the larger miniatures observed in *dor* mutants originate postsynaptically because of a larger glutamate receptor field.

We further tested the presynaptic contribution of Dor to synaptic vesicle release by presynaptically expressing Dor at NMJs of *dor* mutants (v*GlutGAL4*). This condition does not rescue the larger mEJCs that we observed in *dor* mutants. However, compared with *dor* mutants, we find larger EJCs (Fig. 3, A and B) and higher quantal content (Fig. 3, D–F) in *dor* mutants expressing Dor presynaptically. These data indicate that Dor regulates quantal content in a cell-autonomous manner.

To further test the conclusion that fewer vesicles fuse upon stimulation in *dor* mutants, we used FM 1–43 dye labeling of NMJ nerve terminals. Vesicle fusion elicits reformation of new vesicles from the plasma membrane that can be labeled by FM 1–43, providing a measure of presynaptic vesicle cycling. We stimulated *dor* mutants in the presence of FM 1–43 and measured the distribution and amount of dye uptake. FM 1–43 distributes very similar to controls, but the *dor* mutants internalize less dye (Fig. 3, G and H). Indicating specificity, expression of wild-type Dor using *vGlutGAL4* or *daGAL4* at least partially rescues the defect (Fig. 3 H). Hence, loss of *dor* at presynaptic terminals results in reduced vesicle cycling during stimulation.

Next, we probed into the nature of the presynaptic defects observed in *dor* mutants by evaluating synaptic vesicle number, the presence of endocytic intermediates, and the number of vesicles tethered at presynaptic release sites. None of these parameters is affected in *dor* mutants (Fig. S2, B–D), suggesting Dor does not majorly influence vesicle reformation and tethering. We then measured the size of the RRP. We determined the cumulative released number of quanta during a short high frequency stimulation train (60 Hz and 600 ms) and back extrapolated the trend line between 400 and 600 ms (Miskiewicz et al., 2014). We find the RRP is ∼30% smaller in *dor* mutants compared with controls (Fig. 3, I and J), suggesting the defect in quantal content observed in *dor* mutants may be attributed, at least in part, to a smaller RRP. Previous work with mutants that affect the function of the lysosome also show reduced neurotransmitter release (Sweeney and Davis, 2002; Dermaut et al., 2005), but it is not known whether they too affect the RRP.

### Synaptic vesicle protein turnover is slower in *dor* mutants

Our data indicate that reduced lysosomal trafficking, as observed in *dor* mutants, results in a smaller RRP and that the increased neurotransmitter release in *sky* mutants is dependent on normal levels of endolysosomal trafficking. Based on these data, we hypothesize that lysosomal trafficking is needed for synaptic vesicle protein turnover: In our model, defective endolysosomal traffic in *dor* mutants causes the buildup of older vesicle proteins. We surmise that the longer a protein is in use (the older it is), the higher the probability of damage, and we propose that the buildup of old proteins results in a less efficient release apparatus. To test this model, we fused a synaptic vesicle-associated protein (neuronal synaptobrevin [nSyb]) to a fluorescent timer (FT) protein that changes from blue to red emission over time, allowing us to assess protein-pool age. Newly synthesized nSyb is blue, whereas older nSyb is red, and thus the ratio of red to blue fluorescence provides a measure of protein pool age (Fig. 4 H).

We generated flies expressing FT-nSyb under control of *vGlutGAL4* and observe red and blue fluorescence at synapses (Fig. 4, A and B). At NMJs, FT-nSyb labeling is visible in a typical ring-like pattern that colocalizes with the synaptic vesicle marker cysteine string protein (CSP; Fig. 4 C). Furthermore, when the synaptic vesicles are allowed to fuse with the membrane, but their endocytosis is blocked using a temperature-sensitive

and 7 (C) and quantification (D) of patches of FM 1–43 (arrowheads) after 1-min 90 mM KCl stimulation ($n$ = 12–20). (E and F) Traces (E) and quantification (F) of EJCs recorded from larval fillets in HL3 with 0.5 mM $CaCl_2$ in FRT40A controls ($n$ = 7), $sky^{1/2}$ mutants ($n$ = 8), $sky^{1/2}$; *UAS-Rab7*$^{RNAi}$ *nSybGAL4* (*Rab7*$^{RNAi}$; $n$ = 20), and $sky^{1/2}$; *UAS-dVPS39*$^{RNAi}$ *nSybGAL4* (*dVPS39*$^{RNAi}$; $n$ = 12), expressing the RNAi constructs in all neurons. (G and H) Images of FM 1–43 labeling in NMJs on muscle 6 and 7 (G) and quantification (H) of patches of FM 1–43 (arrowheads) after 1-min 90 mM KCl stimulation ($n$ = 12–16). Bars, 5 µm. Error bars: SEM. One-way ANOVA (post hoc Tukey's and Dunnett's test): *, P < 0.05; **, P < 0.01; ***, P < 0.001.

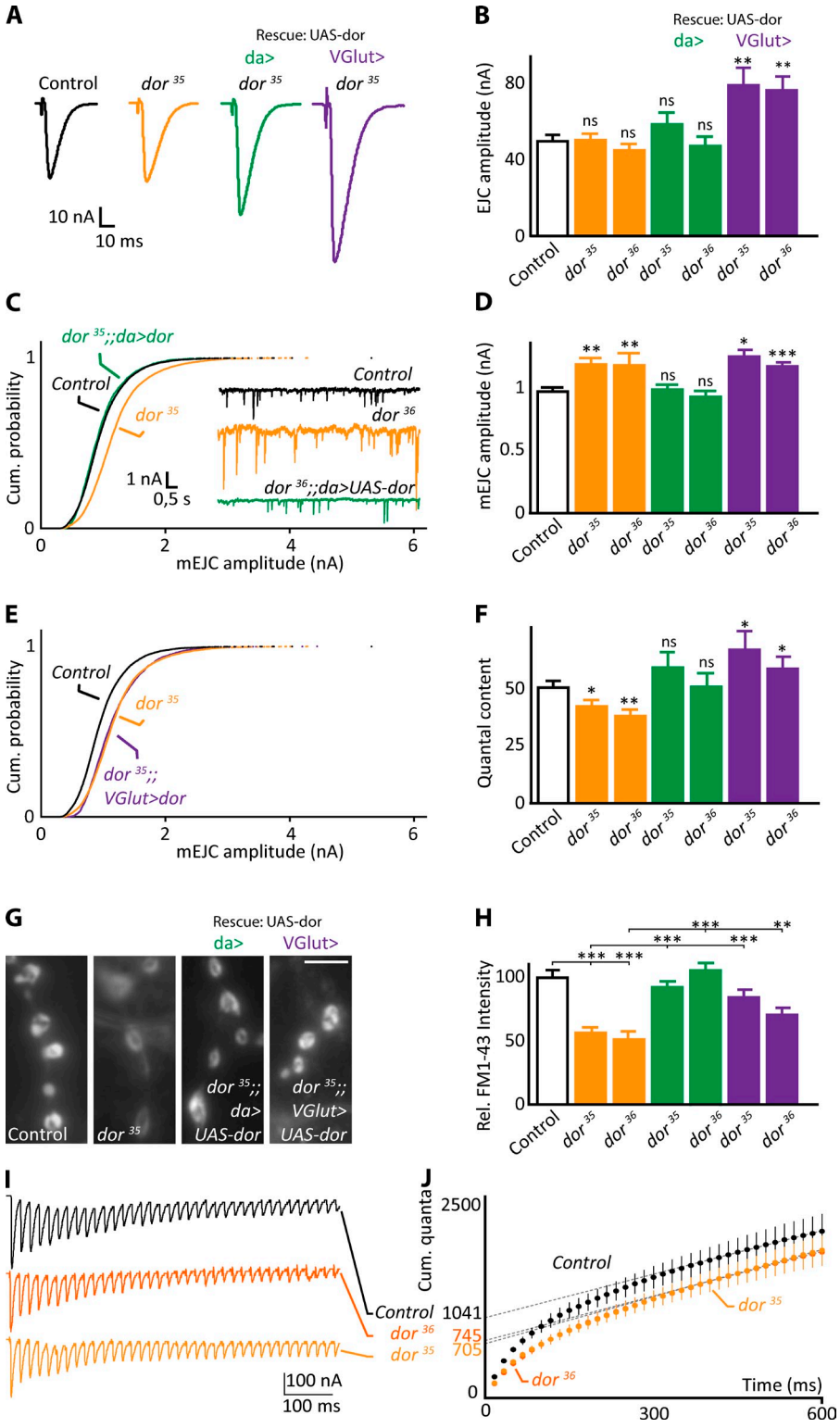


Figure 3. **Loss of *dor* function causes defects in vesicle fusion efficiency.** (A and B) EJCs (A) recorded in HL-3 with 0.5 mM $CaCl_2$ from FRT19A control (white), $dor^{35}$ and $dor^{36}$ (orange), $dor^{35}$ and $dor^{36}$ expressing wild-type Dor ubiquitously (*daGAL4*; green), or presynaptically at the NMJ (*vGlutGAL4*, purple). (B) Quantification of the mean EJC amplitude ($n$ = 8–17). (C–E) mEJCs, cumulative probability mEJC histograms (C and E), and quantification of mean mEJC amplitudes (D; $n$ = 7–15). (F) Quantal content; EJC amplitude/mEJC amplitude (see also A; $n$ = 8–17). For B, D, and F, error bars show SEM, with one-way ANOVA (post hoc Dunnett's test) compared with control: *, P < 0.05; **, P < 0.01; ***, P < 0.001. (G and H) Images of FM 1–43 labeling after 1 min of 90 mM KCl stimulation at larval NMJs (G) and quantification of labeling intensity (H; $n$ = 12–30). Bar, 5 µm. Error bars: SEM. *t* test: **, P < 0.01; ***, P < 0.001. (I and J) Raw data traces of EJC recordings made in HL-3 with 5 mM calcium and stimulated at 60 Hz in FRT19A controls, $dor^{35}$, and $dor^{36}$ mutants (I) and quantification of the cumulative released quantal content in such recordings versus time (J). The y intercept of the slope of the trend line (dotted lines) at steady state (points 400–600 ms) provides a measure of the mean RRP size (indicated on the y axis: control: 1,041 ± 109 quanta; $dor^{36}$: 745 ± 56 quanta; $dor^{36}$: 705 ± 54 quanta; $n$ = 6–8). Error bars: SEM.

*dynamin* ($shi^{ts1}$), the FT-nSyb redistributes more to the presynaptic membrane (Fig. 4 D). These data indicate that FT-nSyb properly localizes to and associates with synaptic vesicles.

We also assessed whether expression of the FT-nSyb affects synaptic function. FT-nSyb–expressing flies survive, can fly, and do not show obvious behavioral defects. In addition, synaptic vesicle cycling in these animals as measured by FM 1–43 dye uptake upon stimulation is similar to controls (Fig. 4, E and F). Thus, expression of the FT-nSyb fusion protein does not overtly affect synaptic function.

Next, we used the FT-nSyb to assess synaptic vesicle protein turnover. First, we tested whether the FT-nSyb is a protein that can be efficiently degraded by fusing it to ubiquitin (Ub), forcing the FT-nSyb to be targeted for degradation. Under identical

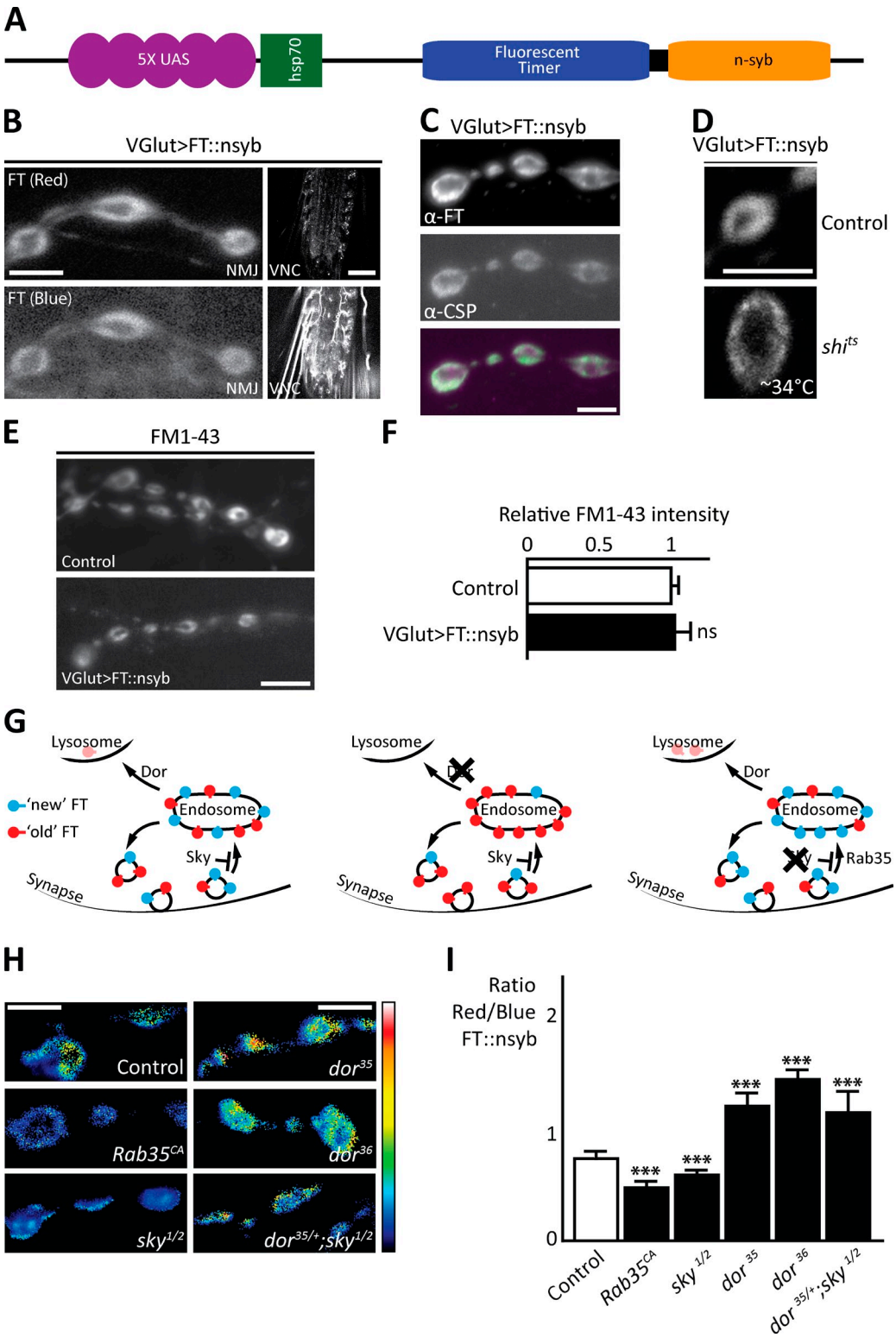


Figure 4. **Synaptic vesicle protein timers reveal slower synaptic vesicle protein turnover in *dor* mutants and faster turnover in *sky* mutants.** (A) Schematic of the FT nSyb construct (FT::nSyb). (B) FT::nSyb expression using *vGlutGAL4* showing the red and blue forms of the timer at the larval NMJ and the ventral nerve cord (VNC). The blue fluorescence is higher than the red in the VNC. (C) NMJ boutons expressing the FT::nSyb using *vGlutGAL4* labeled with antibodies to dsRed (for the FT) and to CSP, a synaptic vesicle protein. (D) FT::nSyb localization (red form) at control boutons and $shi^{ts1}$ mutant boutons stimulated at ~34°C for 10 min using 90 mM KCl. (E and F) Images of FM 1–43 (E) and quantification of labeling intensity (F) at boutons in controls and larva expressing the FT::nSyb using *vGlutGAL4*. (G) Schematic representation of the distribution of the red (old) and blue (young) FT::nSyb in control (left) and *dor* (middle) or *sky* (right) mutants. (H and I) Images (H) and quantification (I) of the ratio of red over blue fluorescence intensities at synaptic boutons shown using the indicated lookup table. FT::nSyb was expressed using *vGlutGAL4* in controls, in animals expressing $Rab35^{CA}$, in $dor^{36}$, $dor^{35}$ and $sky^{1/2}$ mutants as well as in $dor^{35/+}$; $sky^{1/2}$ mutants ($n$ = 20–50). Bars: (B [NMJ], D, and E) 5 µm; (B, VNC) 50 µm; (H) 2 µm. Error bars: SEM. In I, all statistical comparisons are to $dor^{35}$ or $dor^{36}$, except for the double mutant to $sky^{1/2}$. One-way ANOVA (post hoc Tukey's test): ***, $P < 0.0001$.

expression conditions, the synaptic labeling of Ub-FT-nSyb is much lower than that of FT-nSyb, and red fluorescence is almost undetectable (Fig. S3). These results indicate fast and efficient degradation of the ubiquitinated protein. As a further control, we also expressed the FT-nSyb in animals expressing constitutive active Rab35 in which traffic of synaptic vesicles to endosomes is enhanced (Fig. 4 G), and old proteins are expected to be degraded more efficiently (Uytterhoeven et al., 2011). We find a lower red over blue ratio (Fig. 4, H and I), consistent with a younger synaptic vesicle protein pool in $Rab35^{CA}$-expressing animals. We then expressed the FT-nSyb in $dor^{35}$ and $dor^{36}$ mutants and in $sky^{1/2}$ mutants, hypothesizing that older proteins will dwell longer in *dor* mutants and less long in *sky* mutants (Fig. 4 G). In agreement, we find a lower ratio of red-to-blue fluorescence in *sky* mutants and a higher ratio in *dor* mutants (Fig. 4, H and I). Furthermore, this defect in *sky* mutants is reversed when one copy of *dor* is removed (Fig. 4, H and I). Hence, the data are consistent with the idea that Dor-mediated endolysosomal trafficking positively regulates synaptic vesicle protein turnover.

In this work, we establish a fly model of Sky/TBC1D24-induced neurodegeneration and find that reduced function of Dor, a HOPS component, is sufficient to suppress this neurodegeneration. Our data indicate that the synaptic vesicle protein pool in the *sky* mutants is on average younger compared with controls, suggesting excessive degradation of older proteins, thereby promoting synaptic vesicle protein pool rejuvenation. This degradation of older proteins in *sky* mutants is dependent on Dor-mediated endolysosomal trafficking. Indeed, reducing Dor activity results in older, and likely partly dysfunctional proteins, to be kept in the vesicle cycle. Although not directly shown, we surmise that newly synthesized proteins are on average more functional than aged proteins, and these aged proteins may engage in inefficient complexes that dampen the efficacy of neurotransmitter release. Excessive degradation of these older proteins in *sky* mutants indeed correlates with increased neurotransmitter release and with neurodegeneration, both features that are suppressed when partially blocking endolysosomal traffic in the *sky* mutants.

## Materials and methods

### *Drosophila* genetics

All fly stocks were kept on standard corn meal and molasses medium at room temperature. For experiments, mutants and controls were grown in optimal conditions on grape juice plates with fresh yeast paste; except for the FT, light-induced neurodegeneration experiments, and ERG recordings, the controls and the mutants were grown on standard medium. Deficiencies and transgenic stocks (Shestopal et al., 1997; Parks et al., 2004; Dietzl et al., 2007) were obtained from the Bloomington Stock Center Indiana (BL), from Vienna Drosophila RNAi Centre, or were a gift (Sevrioukov et al., 1999). For experiments with $dor^{30}$, $dor^{35}$, and $dor^{36}$ mutants, the controls were *y w P{ry neoFRT}19A* (BL); for *sky* mutants, controls were *y w P{ry⁺ ey-FLP.N}2 P{GMR-LacZ.C(38.1)}TPN1; P{ry⁺ neoFRT}40A* (BL). $dor^{30}$, $dor^{35}$, and $dor^{36}$ are *y w* $dor^{x}$ *P{ry neoFRT}19A*. $sky^{1}$, or $sky^{2}$ is *y w P{ry⁺ ey-FLP.N}2 P{GMR-LacZ.C(38.1)}TPN1;* $sky^{x}$ *P{ry⁺ neoFRT}40A* (Uytterhoeven et al., 2011).

*UAS-dor* is a *dor* cDNA cloned in pUAST inserted on the third chromosome using Δ2,3 transposase (Sevrioukov et al., 1999). *vGlutGal4* and Rab5-GFP (BL) were recombined with $sky^{2}$ using classical genetic techniques and the presence of *{neoFRT}40A* after recombination was not verified.

$dor^{30}$, $dor^{35}$, and $dor^{36}$ (this study) were isolated from an EMS screen for recessive lethal X chromosome mutations with synaptic transmission defects. *y w P{ry neoFRT}19A* (BL) males were fed with EMS, and 12,653 stocks were generated. 2,447 caused X-linked hemizygous lethality in males. We then used mitotic recombination in the fly eye to create female flies with homozygous mutant X chromosomes in their eyes by crossing *y w * P{ry neoFRT}19A/FM7* (* = EMS induced mutations) females to *Df(1)JC70 P{ry neoFRT}19A/Y Dp(1;Y)dx⁺5 y⁺* males and recorded ERGs. *Df(1)JC70* and *Y Dp(1;Y)dx⁺5 y⁺* were obtained from BL. 111 mutants showed consistent ERG defects and were retained. To screen for suppressors of *sky*, flies with homozygous mutant eyes (but heterozygous bodies; Newsome et al., 2000) were generated: Flies with homozygous *sky* eyes *y w P{ry⁺ ey-FLP.N}2 P{GMR-LacZ.C(38.1)}TPN1;* $sky^{2}$ *P{y⁺, ry⁺}25F P{neoFRT}40A/ l(2)cl-2L P{w⁺} P{ry⁺,neoFRT}40A*. Flies with homozygous *sky* eyes and heterozygous for one of the 111 new mutations: *y w P{ry⁺ ey-FLP.N}2 P{GMR-LacZ.C(38.1)}TPN1/y w * P{ry neoFRT}19A;* $sky^{2}$ *P{y⁺, ry⁺}25F P{neoFRT}40A/l(2)cl-2L P{w⁺} P{ry⁺,neoFRT}40A*. Controls were *y w P{ry⁺ ey-FLP.N}2 P{GMR-LacZ.C(38.1)}TPN1; P{y⁺, ry⁺}25F P{neoFRT}40A/l(2)cl-2LP{w⁺} P{ry⁺, neoFRT}40A* (BL) and *y w P{ry⁺ ey-FLP.N}2 P{GMR-LacZ.C(38.1)}TPN1/y w P{ry neoFRT}19A;* $sky^{2}$ *P{y⁺, ry⁺}25F P{neoFRT}40A/ l(2)cl-2L P{w⁺} P{ry⁺,neoFRT}40A* (BL). The ERG profile of these flies was recorded, and the amplitude of on and off transients was quantified.

To identify the lesions in the suppressors of *sky*, we used two strategies to map our mutants. In one approach, we used deficiency and duplication complementation tests, and in the other approach, we used next generation sequencing. To rough map *dor* mutants, we performed a complementation analysis using overlapping deficiencies and duplications obtained from BL. Duplications covering the *dor* region were crossed to *y w* $dor^{x}$ *P{ry neoFRT}19A/FM7c, P{GAL4-Kr.C}DC1, P{UAS-GFP.S65T}DC5, sn[+]*, and rescue of lethality was assessed by the presence of males with normal eyes. These were then used to cross with deficiencies. For whole genome sequencing, genomic DNA of $dor^{35}$ was isolated (see Molecular biology). The list of mutations was analyzed considering the previously acquired genetic mapping. When grown on grape juice plates with fresh yeast paste, *dor* mutants (homozygous and heteroallelic combinations) die as third instar larvae.

### Light-induced neurodegeneration

Greater than 1-d-old flies were collected and exposed to constant white light of 1,300 LUX at 25°C. At the given time points, the flies were further processed for histology.

### Molecular biology

For sequencing of *dor* mutants, genomic DNA was isolated from control and *dor* male larvae *y w P{ry neoFRT}19A* and *y w* $dor^{x}$ *P{ry neoFRT}19A* using the E.Z.N.A. Insect DNA kit (OMEGA Bio-Tek), and ∼500-bp fragments were amplified by PCR using the primers in Table S1. PCR fragments were sequenced with the same primers using Sanger sequencing.

For whole genome sequencing, female flies were collected from both control and heterozygous EMS mutants with the following genotypes: *y w P{ry neoFRT}19A* and *y w* P{ry neoFRT}19A*. DNA was isolated using the E.Z.N.A. Insect DNA kit and RNase (QIAGEN). Sequencing libraries were prepared by ACGT according the manufacturer's protocol. Samples were sequenced with SOLiD (Applied Biosystems) at ∼10× mean coverage. The sequence reads were aligned to the dm3 genome assembly (Berkeley Drosophila Genome Project Release 5) using bowtie (Li and Durbin, 2009; parameters for bowtie are –a, –m3, –best, and –strata), single nucleotide polymorphisms (SNPs) were called using SAMtools (Li et al., 2009) and VarScan (Koboldt et al., 2009), and SNP consequences were obtained using Ensembl's Variant Effect Predictor (McLaren et al., 2010). SNPs common to the control sample as well as to the mutants were removed. The Interactive Genomics Viewer was used for visualization of the SNPs.

Proteins were extracted by crushing control and mutant larvae in lysis buffer (25 mM Hepes, 100 mM NaCl, 1 mM $CaCl_2$, and 0.5% Triton X-100) with protease inhibitor cocktail (Roche) followed by clearing by centrifugation at 10,000 *g* at 4°C for 10 min. Proteins were separated on a Bis-Tris 4–12% precast gels (Life Technologies) and transferred to a nitrocellulose membrane. For labeling the blots, the following primary antibodies were used: guinea pig anti-Dor at 1:500 (a gift from H. Krämer, University of Texas Southwestern, Dallas, TX; Sevrioukov et al., 1999), mouse anti–Cathepsin L mAb at 1:250 (R&D systems), rabbit anti-Acon pAb at 1:5,000 (Abgent), mouse anti–α-Tubulin mAb at 1:2,000 (Sigma-Aldrich). The following secondary antibodies were used: HRP-conjugated anti–mouse (1:10,000; Jackson ImmunoResearch Laboratories, Inc.), anti–rabbit (1:10,000; Jackson ImmunoResearch Laboratories, Inc.), or anti–guinea pig (1:1,000; Dako) IgG antibodies. Blots were developed using Western Lightning ECL or ECL+ (PerkinElmer).

*UAS-FT-nSyb* was generated by chimeric PCR using the primers in Table S1 and making use of the *UAS-nSyb-Ub-pUAST* vector (Uytterhoeven et al., 2011) and a vector with the slow FT (Subach et al., 2009) as

templates. The primers used encoded a 5×(Gln–Ser) spacer between the timer and the nSyb. *UAS-Ub-FT-nSyb* consists of residues 1–74 from fly Ub *Rpl40* fused N-terminally to *nSyb-timer* with the spacer Gln–Gln–Ser–Arg separating Ub and nSyb. The C-terminal glycine residues of Ub were omitted to prevent its removal by deubiquitinases, as previously described (Raiborg et al., 2002). All constructs were cloned into the KpnI and NotI restriction sites of pUASt-attB and sequenced (Bischof et al., 2007). *UAS-FT-nSyb* and *UAS-Ub-FT-nSyb* were inserted into the genome using phi-C-31–mediated transgenesis in the VK31 docking site on the third chromosome (Best Gene).

### RT-PCR

Total RNA was isolated from adult flies expressing UAS-*Vps39* RNAi (Vienna Drosophila RNAi Centre) with a *daGAL4* driver (BL) and from adult fly heads expressing UAS-*Rab7* RNAi (Vienna Drosophila RNAi Centre) with the *nSybGAL4* driver (BL) using Tri Reagent (Sigma-Aldrich) according to the manufacturer's protocol. To prevent DNA contamination, the extracted RNA was digested with RQ1 DNase (Promega), and LiCl was used to precipitate the RNA. Subsequently, cDNA was amplified using the SuperScript III First-Strand Synthesis System (Life Technologies). The SYBR green kit and LightCycler 480 were used for analysis (Roche). The primers listed in Table S1 were used, and the ribosomal protein RP49 was used to normalize the data. RNA quantities were determined using the Δ-Δ-CT method. Threshold cycle values were corrected for amplification efficiency that was determined for each amplicon based on dilution series (1–1:256).

### Histology of retina and brain

Anesthetized adult flies with *white* mutant eye clones were regularly spaced with plain red eyed flies in a fly guillotine to fix their head. Subsequently, the flies were fixed in Carnoy's fix (%):60 ethanol, 30 chloroform, and 10 glacial acetic acid, overnight. After fixation, the flies were embedded in paraffin. The autofluorescence of 7-µm-thick sections was imaged using a confocal microscope (A1R; Nikon), NIS-Elements Advanced Research software (Nikon) and a 20×, 0.75 NA air lens (excitation of 488 nm; emission of 525/50 nm) at room temperature. The areas of the vacuoles and retina were manually encircled using ImageJ (National Institutes of Health) to quantify their surface area, and images were further processed with Photoshop (Adobe).

### Imaging

For immunolabeling, NMJs were dissected in HL-3 (mM): 110 NaCl, 5 KCl, 10 $NaHCO_3$, 5 Hepes, 30 sucrose, 5 trehalose, and 10 $MgCl_2$, pH 7.2, fixed in 3.7% formaldehyde for 20 min (for GluRIIA labeling: Bouin's solution [Sigma-Aldrich]) and washed and permeabilized in PBS with 0.1% Triton X-100. Primary antibodies were added overnight at 4°C. Preparations were then washed again in PBS with Triton X-100 and blocked with 2% normal goat serum for 1 h at room temperature. Secondary antibodies were added to the normal goat serum block solution for 4 h, and samples were washed several times in PBS with Triton X-100 before mounting them in Vectashield (Vector Laboratories, Inc.). Primary antibodies used were mouse anti-CSP mAb at 1:50, anti-GluRIIA at 1:50 (49/92 and 8B4D2; Developmental Studies Hybridoma Bank; Zinsmaier et al., 1990), and rabbit anti-dsRed pAb at 1:500 (Takara Bio Inc.). Secondary antibodies were Alexa Fluor 488 or 647 conjugated (Life Technologies) and used at 1:500. Quantification of labeling intensities was performed using NIS-Elements Basic Research software by encircling areas of interest and measuring the mean pixel intensity. Background labeling in muscles was subtracted, and the data were normalized to the anti-HRP labeling intensity

For FM 1–43, third instar larvae were dissected in HL-3, and motor neurons were cut. Larvae were then stimulated in the presence of 4 µM FM 1–43 (Life Technologies) for 1 min in HL-3 with 90 mM KCl or 12 µM FM 4–64 for 5 min in HL-3 with (mM) 90 KCl, 25 NaCl, 90 KCl, 10 $NaHCO_3$, 5 Hepes, 30 sucrose, 5 trehalose, 10 $MgCl_2$, and 1.5 $CaCl_2$, pH 7.2. Larvae were washed with HL-3 to remove noninternalized dye and imaged. The number of FM 1–43 accumulations per synaptic area was manually assessed by counting the inclusions per NMJ, and this value was normalized over the FM 1–43-labeled NMJ surface area measured in ImageJ. Quantification of labeling intensity was performed by manually encircling the labeled area in ImageJ and calculating the mean pixel intensity within this area, as previously described (Verstreken et al., 2008). Images were processed with Photoshop using background and contrast settings.

To visualize the vesicle pool in $shi^{ts1}$ mutants expressing FT-nSyb, larvae were dissected in HL-3 and stimulated with prewarmed HL-3 with 90 mM for 10 min at ∼34°C. The larvae were then washed with prewarmed HL-3 to relax the preparation. Samples were subsequently live imaged.

Images were captured using a confocal microscope (A1R) for immunohistochemistry, live imaging of $shi^{ts1}$ mutants expressing UAS-FT-nSyb, and the colocalization of FM 4–64 (excitation of 488 nm; emission of 700/75 nm) accumulations with Rab5-GFP (excitation of 488 nm; emission of 525/50 nm), through a 60×, 1.2 NA water immersion lens (immunohistochemistry) or near-infrared Apochromat 60×, 1.0 NA water dipping lens (live imaging and colocalization) at room temperature. Images to analyze FM 1–43 accumulations were acquired using a confocal microscope (510 META; Carl Zeiss) with Zen software and an Achroplan 63×, 0.9 NA water dipping lens at room temperature. Images to assess FM 1–43 labeling intensity were acquired with a fluorescent microscope (Eclipse FN1; Nikon) with a digital camera (C10600 ORCA-R2; Hamamatsu Photonics), NIS-Elements Advanced Research software package, and a 60×, 1.0 NA water dipping lens using excitation of 470/40 nm and emission of BA520 filter block at room temperature. Images were processed with Photoshop using background and contrast settings.

To image the FTs, third instar larval fillets were prepared in HL-3, and the motor neurons were cut. Images were captured using a confocal microscope (AR1), through a near-infrared Apochromat 60×, 1.0 NA water dipping lens at room temperature. Blue and red channels were imaged separately (excitation: blue, 405 nm and red, 561 nm; emission: blue, 450/50 nm and red, 595/50 nm) at room temperature. For ratio calculations, the intensities of the boutons were quantified for both blue and red channels as described in this paragraph, and the ratios were calculated. The ratio images were prepared using the FIJI: both channels were first converted to a 32-bit image and thresholded, retaining only the boutonic labeling; then, the "red" image was divided by the "blue" using the arithmetic module, and a look-up table was applied to the resulting image. As a result, the images only include boutonic areas (the thresholded area), and the rest of the image was intentionally left black.

### Electrophysiology

For ERGs, flies were immobilized with liquid Pritt glue, and a glass recording electrode filled with NaCl was placed on the eye, whereas the reference electrode filled with NaCl was placed in the thorax of the fly (Venken et al., 2008). We used digitally controlled light-emitting diode green light to deliver 1-s light pulses. Data were recorded with Clampex 10.2 (Molecular Devices), and data were quantified in Clampfit 10.2 (Molecular Devices) using maximum and minimum detection. Raw data traces (also for EJCs, see next paragraph) were copied from Clampfit into Canvas 15 (Deneba) and inserted into the figure.

Two electrode voltage clamp recordings in third instar larvae were performed on muscle 6, segment A2, in HL-3 (see Imaging) using <30 MΩ intracellular electrodes (Verstreken et al., 2009). The membrane holding potential was −70 mV, voltage errors were <1.5 mV for 100 nA EJCs, and input resistances were ≥5 MΩ. All data were filtered at 1 kHz (miniatures at 600 Hz). Synaptic currents or membrane potentials were monitored with an amplifier (Axoclamp 900A; Molecular Devices) and digitized using a Digidata 1440A (Molecular Devices). EJCs in 0.5 mM external calcium were evoked by stimulation of the cut segmental nerve at 2× threshold. mEJCs were recorded in 0.5 mM $CaCl_2$. To determine the RRP size using the cumulative quantal content method, motor neurons were stimulated at 60 Hz for 600 ms in HL-3 with 5 mM $CaCl_2$. EJC amplitudes are plotted as cumulative quantal content. The trend line slope through points at 400–600 ms is a measure for the RRP refilling rate, and the y-intercept corresponds to the RRP size (Habets and Borst, 2007). Basal EJC amplitudes were determined in Clampfit 10.2 by calculating the mean of 60 traces. mEJC amplitudes were quantified using the event detection module in Clampfit 10.2 and calculated from 5-min recordings. Quantal content was determined by dividing the mean EJC amplitude by the mean mEJC amplitude.

### TEM

For TEM, larvae were dissected in HL-3 and fixed immediately in 1% glutaraldehyde, 4% paraformaldehyde, and 1 mM $MgCl_2$ in 0.1 M Na-cacodylate buffer, pH 7.4. Subsequently, specimens were osmicated in $OsO_4$/Na-cacodylate buffer for 2 h and stained in 2% aqueous uranyl acetate (1.5 h). After dehydration using a series of ethanol, specimens were embedded in Agar 100 (Laborimpex; Agar Scientific). Ultrathin sections (60–70 nm) were cut with an ultramicrotome (EM UC7; Leica), collected on grids (Laborimpex; Agar Scientific), and coated with Butvar. Sections were imaged using a transmission electron microscope (JEM 1400; JEOL) at 80 kV. Micrographs were acquired using a bottom-mounted camera (Quemesa; 11 megapixels; Olympus) using iTEM 5.2 software (Olympus). Ultrastructural features were quantified with ImageJ from boutonic profiles whose surface area is ≥1 $µm^2$. Diameters of synaptic vesicles were measured

from profiles with clearly visible membranes. EM micrographs were processed in Photoshop using brightness and contrast.

**Online supplemental material**

Fig. S1 shows the genetics and molecular biology that led to the identification of the three novel mutations in *dor*. Fig. S2 shows the colocalization between FM accumulations in *dor/+; sky* mutants and Rab5-GFP as well as EM analysis of *dor* mutant synaptic boutons. In Fig. S3, the characterization of the FT-nSyb chimera fused to Ub is shown. Table S1 shows a list of the primers used in this study. Online supplemental material is available at http://www.jcb.org/cgi/content/full/jcb.201406026/DC1.

We thank the Bloomington and Vienna fly stock centers and the Developmental Studies Hybridoma Bank; H. Krämer, B. De Strooper, J De Wit, B. Hassan, J. McInnes, G. Hulselmans, Z. Kalender N. Corthout, S. Munck (VIB BioImaging Core and Light Microscopy Network), P. Baatsen (KU Leuven EM core), and members of the Verstreken laboratory for reagents and/or help.

Support to P. Verstreken was from an European Research Council Starting Grant (260678), the Fonds voor Wetenschappelijk Onderzoek Vlaanderen (G053913N, G079013N, G095511N, G094011N, and a fellowship to VU), the Hercules Foundation, Instituut voor Wetenschap en Technologie (a fellowship to J.R. Slabbaert), an Interuniversitaire Attractie Pool by the Belgian Science Policy, the research fund KU Leuven, and a Methusalem grant of the Flemish government and VIB.

The authors declare no competing financial interests.

Submitted: 6 June 2014
Accepted: 22 October 2014

## References

Bischof, J., R.K. Maeda, M. Hediger, F. Karch, and K. Basler. 2007. An optimized transgenesis system for *Drosophila* using germ-line-specific phiC31 integrases. *Proc. Natl. Acad. Sci. USA*. 104:3312–3317. http://dx.doi.org/10.1073/pnas.0611511104

Campeau, P.M., D. Kasperaviciute, J.T. Lu, L.C. Burrage, C. Kim, M. Hori, B.R. Powell, F. Stewart, T.M. Félix, J. van den Ende, et al. 2014. The genetic basis of DOORS syndrome: an exome-sequencing study. *Lancet Neurol.* 13:44–58. http://dx.doi.org/10.1016/S1474-4422(13)70265-5

Corbett, M.A., M. Bahlo, L. Jolly, Z. Afawi, A.E. Gardner, K.L. Oliver, S. Tan, A. Coffey, J.C. Mulley, L.M. Dibbens, et al. 2010. A focal epilepsy and intellectual disability syndrome is due to a mutation in TBC1D24. *Am. J. Hum. Genet.* 87:371–375. http://dx.doi.org/10.1016/j.ajhg.2010.08.001

Dermaut, B., K.K. Norga, A. Kania, P. Verstreken, H. Pan, Y. Zhou, P. Callaerts, and H.J. Bellen. 2005. Aberrant lysosomal carbohydrate storage accompanies endocytic defects and neurodegeneration in *Drosophila benchwarmer*. *J. Cell Biol.* 170:127–139. http://dx.doi.org/10.1083/jcb.200412001

Dietzl, G., D. Chen, F. Schnorrer, K.-C. Su, Y. Barinova, M. Fellner, B. Gasser, K. Kinsey, S. Oppel, S. Scheiblauer, et al. 2007. A genome-wide transgenic RNAi library for conditional gene inactivation in *Drosophila*. *Nature*. 448:151–156. http://dx.doi.org/10.1038/nature05954

Falace, A., F. Filipello, V. La Padula, N. Vanni, F. Madia, D. De Pietri Tonelli, F.A. de Falco, P. Striano, F. Dagna Bricarelli, C. Minetti, et al. 2010. TBC1D24, an ARF6-interacting protein, is mutated in familial infantile myoclonic epilepsy. *Am. J. Hum. Genet.* 87:365–370. http://dx.doi.org/10.1016/j.ajhg.2010.07.020

Fernández-Chacón, R., M. Wölfel, H. Nishimune, L. Tabares, F. Schmitz, M. Castellano-Muñoz, C. Rosenmund, M.L. Montesinos, J.R. Sanes, R. Schneggenburger, and T.C. Südhof. 2004. The synaptic vesicle protein CSP α prevents presynaptic degeneration. *Neuron*. 42:237–251. http://dx.doi.org/10.1016/S0896-6273(04)00190-4

Guven, A., and A. Tolun. 2013. TBC1D24 truncating mutation resulting in severe neurodegeneration. *J. Med. Genet.* 50:199–202. http://dx.doi.org/10.1136/jmedgenet-2012-101313

Habets, R.L., and J.G. Borst. 2007. Dynamics of the readily releasable pool during post-tetanic potentiation in the rat calyx of Held synapse. *J. Physiol.* 581:467–478. http://dx.doi.org/10.1113/jphysiol.2006.127365

Koboldt, D.C., K. Chen, T. Wylie, D.E. Larson, M.D. McLellan, E.R. Mardis, G.M. Weinstock, R.K. Wilson, and L. Ding. 2009. VarScan: variant detection in massively parallel sequencing of individual and pooled samples. *Bioinformatics*. 25:2283–2285. http://dx.doi.org/10.1093/bioinformatics/btp373

Li, H., and R. Durbin. 2009. Fast and accurate short read alignment with Burrows-Wheeler transform. *Bioinformatics*. 25:1754–1760. http://dx.doi.org/10.1093/bioinformatics/btp324

Li, H., B. Handsaker, A. Wysoker, T. Fennell, J. Ruan, N. Homer, G. Marth, G. Abecasis, and R. Durbin. 1000 Genome Project Data Processing Subgroup. 2009. The Sequence Alignment/Map format and SAMtools. *Bioinformatics*. 25:2078–2079. http://dx.doi.org/10.1093/bioinformatics/btp352

McLaren, W., B. Pritchard, D. Rios, Y. Chen, P. Flicek, and F. Cunningham. 2010. Deriving the consequences of genomic variants with the Ensembl API and SNP Effect Predictor. *Bioinformatics*. 26:2069–2070. http://dx.doi.org/10.1093/bioinformatics/btq330

Milh, M., A. Falace, N. Villeneuve, N. Vanni, P. Cacciagli, S. Assereto, R. Nabbout, F. Benfenati, F. Zara, B. Chabrol, et al. 2013. Novel compound heterozygous mutations in TBC1D24 cause familial malignant migrating partial seizures of infancy. *Hum. Mutat.* 34:869–872. http://dx.doi.org/10.1002/humu.22318

Miskiewicz, K., L.E. Jose, W.M. Yeshaw, J.S. Valadas, J. Swerts, S. Munck, F. Feiguin, B. Dermaut, and P. Verstreken. 2014. HDAC6 is a Bruchpilot deacetylase that facilitates neurotransmitter release. *Cell Reports*. 8:94–102. http://dx.doi.org/10.1016/j.celrep.2014.05.051

Narayanan, R., H. Krämer, and M. Ramaswami. 2000. *Drosophila* endosomal proteins hook and deep orange regulate synapse size but not synaptic vesicle recycling. *J. Neurobiol.* 45:105–119. http://dx.doi.org/10.1002/1097-4695(20001105)45:2<105::AID-NEU5>3.0.CO;2-X

Newsome, T.P., B. Asling, and B.J. Dickson. 2000. Analysis of *Drosophila* photoreceptor axon guidance in eye-specific mosaics. *Development*. 127:851–860.

Parks, A.L., K.R. Cook, M. Belvin, N.A. Dompe, R. Fawcett, K. Huppert, L.R. Tan, C.G. Winter, K.P. Bogart, J.E. Deal, et al. 2004. Systematic generation of high-resolution deletion coverage of the *Drosophila melanogaster* genome. *Nat. Genet.* 36:288–292. http://dx.doi.org/10.1038/ng1312

Raiborg, C., K.G. Bache, D.J. Gillooly, I.H. Madshus, E. Stang, and H. Stenmark. 2002. Hrs sorts ubiquitinated proteins into clathrin-coated microdomains of early endosomes. *Nat. Cell Biol.* 4:394–398. http://dx.doi.org/10.1038/ncb791

Rieder, S.E., and S.D. Emr. 1997. A novel RING finger protein complex essential for a late step in protein transport to the yeast vacuole. *Mol. Biol. Cell*. 8:2307–2327. http://dx.doi.org/10.1091/mbc.8.11.2307

Sevrioukov, E.A., J.P. He, N. Moghrabi, A. Sunio, and H. Krämer. 1999. A role for the deep orange and carnation eye color genes in lysosomal delivery in *Drosophila*. *Mol. Cell*. 4:479–486. http://dx.doi.org/10.1016/S1097-2765(00)80199-9

Shestopal, S.A., I.V. Makunin, E.S. Belyaeva, M. Ashburner, and I.F. Zhimulev. 1997. Molecular characterization of the deep orange (dor) gene of *Drosophila melanogaster*. *Mol. Gen. Genet.* 253:642–648. http://dx.doi.org/10.1007/s004380050367

Stowers, R.S., and T.L. Schwarz. 1999. A genetic method for generating *Drosophila* eyes composed exclusively of mitotic clones of a single genotype. *Genetics*. 152:1631–1639.

Subach, F.V., O.M. Subach, I.S. Gundorov, K.S. Morozova, K.D. Piatkevich, A.M. Cuervo, and V.V. Verkhusha. 2009. Monomeric fluorescent timers that change color from blue to red report on cellular trafficking. *Nat. Chem. Biol.* 5:118–126. http://dx.doi.org/10.1038/nchembio.138

Sweeney, S.T., and G.W. Davis. 2002. Unrestricted synaptic growth in spinster-a late endosomal protein implicated in TGF-β-mediated synaptic growth regulation. *Neuron*. 36:403–416. http://dx.doi.org/10.1016/S0896-6273(02)01014-0

Uytterhoeven, V., S. Kuenen, J. Kasprowicz, K. Miskiewicz, and P. Verstreken. 2011. Loss of skywalker reveals synaptic endosomes as sorting stations for synaptic vesicle proteins. *Cell*. 145:117–132. http://dx.doi.org/10.1016/j.cell.2011.02.039

Venken, K.J., J. Kasprowicz, S. Kuenen, J. Yan, B.A. Hassan, and P. Verstreken. 2008. Recombineering-mediated tagging of *Drosophila* genomic constructs for in vivo localization and acute protein inactivation. *Nucleic Acids Res.* 36:e114. http://dx.doi.org/10.1093/nar/gkn486

Verstreken, P., T. Ohyama, and H.J. Bellen. 2008. FM 1-43 labeling of synaptic vesicle pools at the *Drosophila* neuromuscular junction. *Methods Mol. Biol.* 440:349–369. http://dx.doi.org/10.1007/978-1-59745-178-9_26

Verstreken, P., T. Ohyama, C. Haueter, R.L. Habets, Y.Q. Lin, L.E. Swan, C.V. Ly, K.J. Venken, P. De Camilli, and H.J. Bellen. 2009. Tweek, an evolutionarily conserved protein, is required for synaptic vesicle recycling. *Neuron*. 63:203–215. http://dx.doi.org/10.1016/j.neuron.2009.06.017

Wucherpfennig, T., M. Wilsch-Bräuninger, and M. González-Gaitán. 2003. Role of *Drosophila* Rab5 during endosomal trafficking at the synapse and evoked neurotransmitter release. *J. Cell Biol.* 161:609–624. http://dx.doi.org/10.1083/jcb.200211087

Zhang, L., R. Sheng, and Z. Qin. 2009. The lysosome and neurodegenerative diseases. *Acta Biochim. Biophys. Sin. (Shanghai)*. 41:437–445. http://dx.doi.org/10.1093/abbs/gmp031

Zinsmaier, K.E., A. Hofbauer, G. Heimbeck, G.O. Pflugfelder, S. Buchner, and E. Buchner. 1990. A cysteine-string protein is expressed in retina and brain of *Drosophila*. *J. Neurogenet.* 7:15–29. http://dx.doi.org/10.3109/01677069009084150